RESEARCH ARTICLE

Sorting and recognition of orbital angular momentum modes through a rotating scattering medium

JinJiang Wang,[1] Hongyu Yan,[1] Yu Lei,[1] Yutian Liang,[1] Ruijian Li,[1] Tong Liu,[1,†] Zhengliang Liu,[2]

Ziyan Huang,[1] Yuan Ren[2,‡]

[1]Department of Aerospace Science and Technology, Space Engineering University, Beijing 101416, China

[2]Department of Basic Course, Space Engineering University, Beijing 101416, China

Corresponding authors. E-mail: †liutong719@163.com, ‡renyuan_823@aliyun.com

Received January 21, 2026; accepted May 6, 2026

Supporting Information

This document provides supplementary information to Sorting and Recognition of Orbital Angular Momentum modes through a rotating scattering medium. We provide detailed information on Note 1: Fitting methods for r_n and Δl at different propagation distances. Note 2: Exploring the convenient relationship between CCR radius, propagation distance, and topological charge difference. Note 3: Validation of NCCS algorithm screening and CCR information extraction analysis. Note 4: Speckle cross-correlation analysis when the test speckle receiving position and the reference speckle receiving position are not at the same position. Note 5: Analysis of speckle cross-correlation at different rotational speeds. Note 6: Analysis of speckle correlation at different propagation distances.

Supplement Note 1: Fitting methods for r_n and Δl at different propagation distances

The fitted data are derived from the numerical simulations in Fig. 4 of Chapter 3 in the main text, with simulation parameters identical to those in the main text: the roughness parameters are $\beta = 50\lambda, \sigma = \lambda$, the refractive index of 1.517, Δl ranges from 1 to 16, and the propagation distances are set to 50 mm, 60 mm, and 70 mm, respectively. Taking the propagation distance of 50 mm as an example, for each Δl corresponding to r_n, 10 independent simulations were conducted and their average values were taken. The corresponding r_n for Δl ranging from 1 to 16 were gradually obtained as raw data to ensure the reliability of the fitted data. The fitting model is based on Equation 10 in the main text, establishing the relationship to be fitted as $r_n = \delta\Delta l + \varepsilon\Delta l^{1/3} + \varsigma$, where δ , ε, and ς are the parameters to be fitted. The fitting relationship is entirely consistent with the physical meaning of the analytical theory, avoiding empirical fitting without physical significance and ensuring the rationality of the fit. The data fitting was performed using OriginPro software, employing a nonlinear curve-fitting algorithm to fit the simulation data. The fitting information and uncertainty analysis results are presented in Table 1.

Table 1 Fitting parameters at different propagation distances.

		Value	Standard deviation	R^2	RMSE
r_n: 50mm	δ	39.242	0.811	0.991	13.11
	ε	15.21	4.09	0.99	
	ς	19.575	7.585	0.951	
r_n: 60mm	δ	45.417	0.305	0.989	14.526
	ε	31.407	6.753	0.998	
	ς	10.85	9.871	0.993	
r_n: 70mm	δ	47.828	0.197	0.989	15.911
	ε	82.484	8.945	0.997	
	ς	-33.949	11.353	0.993	

Among them, R^2 is the coefficient of determination, an important statistical indicator for evaluating the predictive performance of the model. RMSE stands for root mean square error, representing the average deviation between fitted predicted values and actual measured values.

We compared the fitted curve with a propagation distance of 50 mm against the actual simulation data (Δl:1, 3, 5, 7, 9, 11). The simulation conditions were consistent with those in Fig. 4 of the main text, and the results are shown in Table 2.

Table 2 Comparison of simulated and fitted values of r_n at a propagation distance of 50 mm.

	Simulated value (μm)	Fitted value (μm)	Absolute residual (μm)	Relative residual
1	90.524	74.027	16.497	18.22%
3	172.869	159.238	13.631	7.89%
5	256.142	241.794	14.348	5.6%
7	337.235	323.365	13.87	4.11%
9	416.651	404.391	12.26	2.94%
11	498.854	485.063	13.791	2.76%

Based on Tables 1 and 2, it can be seen that the average relative residuals between the above fitting results and the actual simulation data are approximately 6.92%, which validates the rationality and applicability of the data fitting.

Supplement Note 2: Exploring the convenient relationship between CCR radius, propagation distance, and topological charge difference

To explore a more convenient relationship among the CCR radius, propagation distance, and topological charge difference, it can be derived from Section 2 that the CCR radius (r_n) is positively correlated with Δl. Combining this theoretical model with the simulation data from Fig. 4 in Section 3 of the main text, further data fitting was performed for the CCR radius ($r_n(\Delta l, z)$) at different distances (z). The fitting model is based on Equation 10 in the main text, establishing the relationship to be fitted as: $r_n(\Delta l, z) = \delta(z) \cdot \Delta l + \varepsilon(z) \cdot \Delta l^{1/3} + \varsigma(z)$, where

$\delta(z) = p_1 \cdot z^2 + p_2 \cdot z + p_3$, $\varepsilon(z) = q_1 \cdot z^2 + q_2 \cdot z + q_3$, $\varsigma(z) = s_1 \cdot z^2 + s_2 \cdot z + s_3$, $p_1, p_2, p_3, q_1, q_2, q_3, s_1, s_2, s_3$, are the coefficients to be fitted, all of which are constants. The final data fitting plot is shown in Fig 1, and the fitting results for each parameter are presented in Table 3.

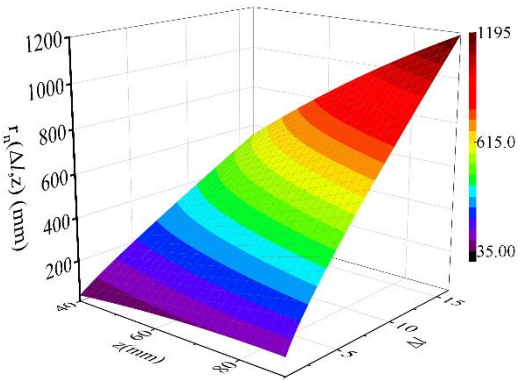

Fig. 1 Fitted surface plot of $r_n(\Delta l, z)$ versus Δl and z.

Table 3 Fitting parameters for $r_n(\Delta l, z)$ with Δl and z.

		Value	Standard deviation	R^2	RMSE
$r_n(\Delta l, z)$	p_1	-0.019	0.006	0.999	33.25
	p_2	2.67	0.825	0.999	
	p_3	-47.689	25.77	0.999	
	q_1	0.171	0.066	0.998	
	q_2	-17.166	8.699	0.998	
	q_3	447.701	271.69	0.999	
	s_1	-0.176	0.078	0.999	
	s_2	18.393	10.29	0.997	
	s_3	-427.756	321.43	0.999	

Based on the above fitting results, we can establish a more convenient relationship among the CCR radius, propagation distance, and topological charge difference. However, since the expression $r_n(\Delta l, z) = \delta(z)\cdot\Delta l + \varepsilon(z)\cdot\Delta l^{1/3} + \varsigma(z)$ is in a bivariate parametric form, when $r_n(\Delta l, z)$ is determined, the propagation distance z must still be known in advance to complete the inversion solution for Δl.

Supplement Note 3: Validation of NCCS algorithm screening and CCR information extraction analysis

In the main text, we select high-correlation speckles based on set thresholds to achieve OAM information extraction. First, to demonstrate that the NCCS algorithm can successfully screen out highly correlated speckle pairs within the optical memory effect range, we conducted the following experimental verification. According to the classical scattering theory of Gaussian random rough surfaces and the analytical model of the optical memory effect, it is known that within a small angular mismatch range, the outgoing speckle fields exhibit strong correlation, with the allowable angular mismatch $\Delta\theta$ as follows (refer to reference [54-56] in the main text):

$$\Delta\theta = \frac{\lambda}{2\pi d}\cdot\frac{\beta}{\sqrt{2}(n-1)\sigma},$$

among them, λ is the wavelength, d is the thickness of the scattering medium, n is the refractive index of the scattering medium, and β and σ are the transverse correlation length and root mean square height of the scattering medium, respectively. The experiment utilized ground glass diffusers (grit size of 220, scattering medium properties: $\lambda = 632.8nm, \beta = 50\lambda, \sigma = \lambda$, d=2 mm, refractive index is 1.517) with a rotation speed of 0.01 rpm and a camera exposure time of 0.01 s, receiving distance of 50 mm. According to the aforementioned theoretical relationship, the theoretical value of $\Delta\theta$ is $0.197°$. In the experiment, we conducted a statistical analysis on the collected speckles: two sets of speckle libraries were acquired, namely the test speckle library ($l_U = 8$) and the reference speckle library ($l_U = 2$), each containing 5,000 speckle images captured at random rotation angles. Before screening, the rotation angle distributions of the scattering media corresponding to the test speckle library and the reference speckle library are shown in Fig. 2 (green for test speckles, red for reference speckles). It can be observed that the rotation angles exhibit a completely random distribution. The NCCS threshold was set at 0.217. The rotation angle distribution after screening by the NCCS algorithm is shown in Fig. 3, while the difference distribution of rotation angles for highly correlated speckle pairs is presented in Fig. 4. The experimental results show that the vast majority of speckle pairs screened by the NCCS algorithm fall within the $\Delta\theta$ range allowed by the optical memory effect, demonstrating that the NCCS algorithm can effectively identify correlated speckle pairs with rotation angles within the optical memory effect range.

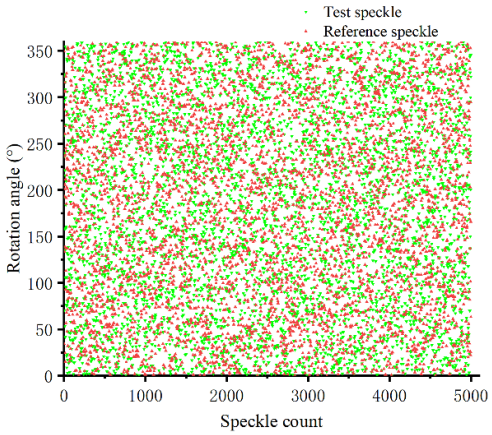

Fig. 2 Rotation angle before screening.

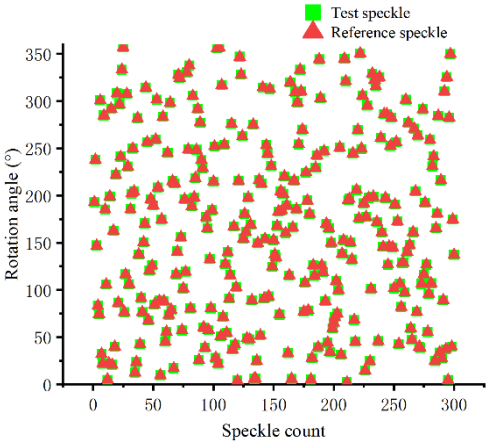

Fig. 3 Rotation angle after screening.

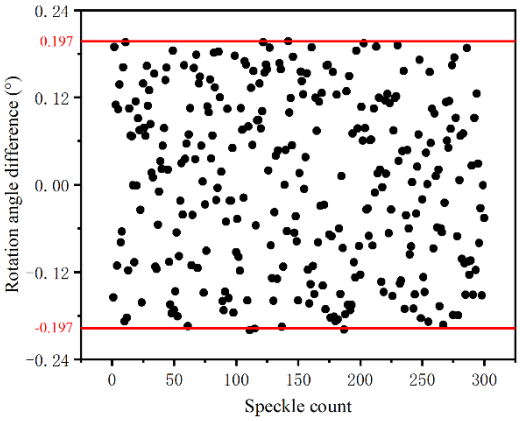

Fig. 4 Rotation angle difference of highly correlated speckle pairs.

Secondly, to investigate the effect of different thresholds on the screening of highly correlated speckles. For the same set of test and reference speckle libraries, thresholds were set at 0, 0.05, 0.1, 0.15, 0.2, 0.21, 0.215, 0.217, and 0.219, respectively. Highly correlated speckles were screened based on each threshold, and the CCR was calculated using the algorithm proposed in the main text, as shown in Fig. 5.

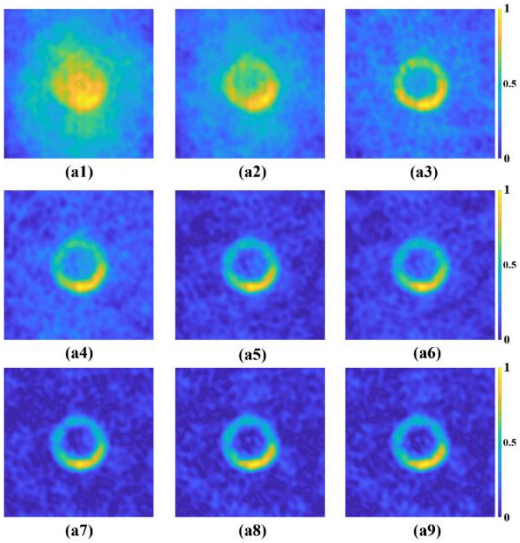

Fig. 5 (a) Extract CCR information based on different thresholds. (a1) 0, (a2) 0.05, (a3) 0.1, (a4) 0.15, (a5) 0.2, (a6) 0.21, (a7) 0.215, (a8) 0.217, (a9) 0.219.

The results show that without NCCS screening, a large number of irrelevant speckles act as noise, significantly reducing correlation. By selecting an appropriate threshold, high-correlation speckles can be effectively filtered out, enabling the extraction of CCR features using the method described in the main text, thereby achieving effective identification of OAM information.

Supplement Note 4: Speckle cross-correlation analysis when the test speckle receiving position and the reference speckle receiving position are not at the same position

The experiment used ground glass diffusers (grit size of 220) as the scattering medium, with the rotation speed set to 0.01 rpm, and the measurement target as $l_U = 8$, reference as $l_U = 2$, and the exposure time is 0.01s. The positions for the test and reference speckle reception were defined such that when they coincided, the position was marked as (0 mm, 0 mm).

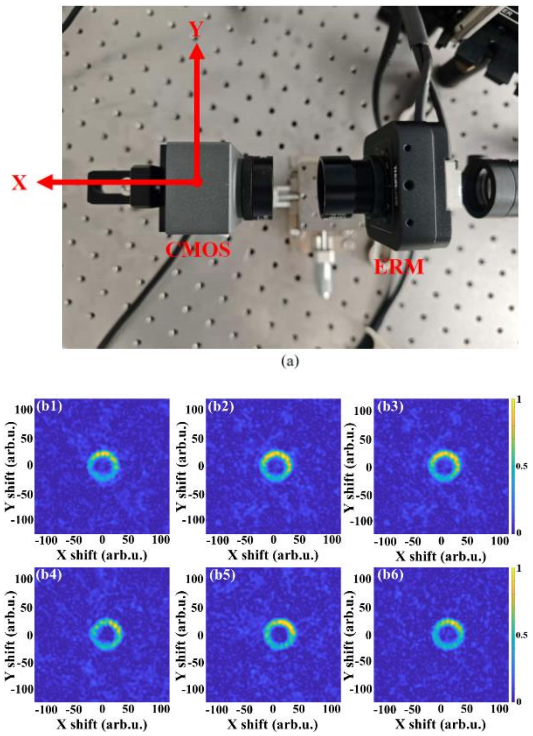

Fig. 6 (a) Position offset schematic diagram. (b) CCR analysis under different positional offsets. b1 (0 mm, 0.05 mm), b2 (0 mm, 0.1 mm), b3 (0 mm, 0.15 mm), b4 (0 mm, 0.2 mm), b5 (0 mm, 0.25 mm), and b6 (0 mm, 0.3 mm).

To verify whether the cross-correlation characteristics of speckles remain significant under slight spatial offsets, the reference speckle reception was fixed at (0 mm, 0 mm), while the test speckle reception position was sequentially translated along the y-axis to (0 mm, 0.05 mm), (0 mm, 0.1 mm), (0 mm, 0.15 mm), (0 mm, 0.2 mm), (0 mm, 0.25 mm), and (0 mm, 0.3 mm) to capture the test speckle patterns, while keeping all other experimental parameters consistent with those in the main text. A schematic of the coordinates is shown in Fig. 6(a). Subsequently, the algorithm proposed in the manuscript was used to extract cross-correlations from the speckle sequences under each offset condition. The experimental results, as shown in Fig. 6(b), demonstrate that even when there is a slight offset between the test and reference speckle reception positions, OAM information can still be extracted using speckle correlation.

Supplement Note 5： Analysis of speckle cross-correlation at different rotational speeds

In the main text, we set a rotating ground glass diffusers at a speed of 0.01 rpm and used a high-speed camera to randomly capture a series of discrete speckle patterns, achieving speckle cross-correlation information extraction. To verify that the method proposed in the main text can still extract OAM information at different rotational speeds, we employed a ground glass diffusers (grit size of 220) sheet as the scattering medium, with the test as $l_U = 8$ and the reference as $l_U = 2$, at rotation speeds of 0.02 rpm, 0.04 rpm, 0.06 rpm, 0.08 rpm, 0.1 rpm, and 0.12 rpm, and the exposure time is 0.01s, while keeping all other experimental parameters consistent with those in the main text. Subsequently, we applied the algorithm proposed in the main text to perform cross-correlation extraction on the speckle sequences under different rotational speeds. The experimental results are shown in Fig. 7. Based on these results, it can be concluded that even when the rotation speed of the ground glass diffusers varies, as long as clear speckle patterns can be captured, the method proposed in the main text can still be used to extract OAM information.

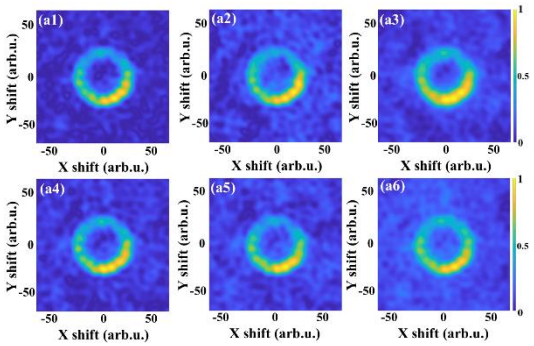

Fig. 7 CCR analysis at different rotational speeds. (a1) 0.02rpm, (a2) 0.04rpm, (a3) 0.06rpm, (a4) 0.08rpm, (a5) 0.1rpm, (a6) 0.12rpm.

Supplement Note 6: Analysis of speckle correlation at different propagation distances

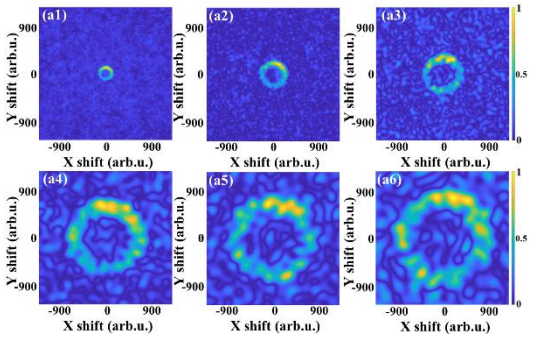

Fig. 8 CCR analysis at different propagation distances. (a1) 150mm, (a2) 200mm, (a3) 250mm, (a4) 300mm, (a5) 350mm, (a6) 400mm.

The experiment used ground glass diffusers (grit size of 220) as the scattering medium, with the rotation speed set at 0.01 rpm, with the test as $l_U = 8$ and the reference as $l_U = 2$, and the exposure time is 0.01s. Speckle patterns at

distances of 150mm, 200mm, 250 mm, 300 mm, 350 mm, and 400 mm were measured respectively. After processing with the algorithm described in the main text, the CCR at different distances could be obtained. The experimental results are shown in Fig. 8, demonstrating that even at longer propagation distances, the cross-correlation between speckles can still be effectively utilized.